

## H-atom ionization by elliptically polarized microwave fields: The overlap criterion

Krzysztof Sacha and Jakub Zakrzewski

*Instytut Fizyki imienia Mariana Smoluchowskiego, Uniwersytet Jagielloński, ulica Reymonta 4, 30-059 Kraków, Poland*

(Received 11 February 1997)

The threshold for H-atom ionization by elliptically polarized microwave fields is discussed within the classical-mechanics framework using the Chirikov overlap criterion. It is shown that the trends observed in the recent experiment [M. R. W. Bellerma *et al.* Phys. Rev. Lett. **76**, 892 (1996)] are qualitatively reproduced by the theory; the origin of the remaining discrepancy is discussed. Increased stability of some orbits with respect to the perturbation due to the elliptically polarized microwaves has been related to vanishing widths of the corresponding resonance islands. Analytic Chirikov overlap prediction is compared with results of numerical simulations. [S1050-2947(97)04207-8]

PACS number(s): 32.80.Rm, 32.80.Wr, 32.80.Fb, 05.45.+b

### I. INTRODUCTION

The ionization of hydrogen atoms by linearly polarized (LP) microwaves has been intensively studied for more than 20 years (for a recent review see [1]). Similarly, a considerable understanding of the effects induced by circularly polarized (CP) radiation is now available [2]. By far much less is known for the general case of elliptically polarized (EP) microwaves. Until very recently the studies considered only the dependence of the ionization threshold on the microwave polarization in the regime of low frequencies (i.e., when the microwave frequency  $\omega \ll \omega_K$ , where  $\omega_K$  is the Kepler frequency corresponding to the initial atomic state). Here experimental results for alkali-metal atoms [3,4] have been reproduced by classical simulations [5]. The regime of high frequencies has been partially discussed within the framework of quantum localization theory using the so-called Kepler map [6]. This approach, however, has been questioned (at least for the limiting case of CP microwaves) by Nauenberg [7]. Similarly, quantum-numerical simulations [2] have shown the limitation of the Kepler map approach applied to CP microwaves.

In view of the very few results available, the recent study of Bellerma *et al.* group [8] may be a cornerstone triggering the investigation of the EP case, a situation somewhat more complicated than the limiting cases of both the LP and the CP cases. In the former case the conservation of the angular momentum projection onto the polarization axis  $L_z$  makes the dynamics effectively two dimensional. In the latter situation, while  $L_z$  is not conserved, the transformation to the frame rotating with the microwave frequency removes the explicit oscillatory time dependence [2]. Both these simplifications are no longer possible in the general EP microwave field and the problem becomes truly multidimensional, providing new challenges to the theory.

Despite these basic differences between the various polarization cases, the experimental results [8] reveal a similarity between the ionization threshold behavior as a function of the scaled frequency  $\omega_0 = \omega/\omega_K$  in the vicinity of the primary resonance between the driving field and the Kepler motion, i.e., for  $\omega_0 \in [0.6, 1.4]$ , provided the microwave field amplitude is appropriately rescaled. The experimental data are quite faithfully reproduced by classical fully three-

dimensional (3D) simulations; moreover, as briefly described by Bellerma *et al.* [8], the polarization independence of the threshold may be understood by a classical analysis of the pendulum Hamiltonian, which is valid in the vicinity of the primary resonance.

Bellerma *et al.* point out, however, that at microwave amplitudes higher than the 10% ionization threshold, e.g., values that lead to 50% ionization, the polarization of the microwave field becomes more important. Specifically, the ionization yield  $P(F)$  as a function of the microwave maximal amplitude  $F$  increases slower for CP than for LP radiation [8]. The ionization threshold (i.e.,  $F$  value leading to a given, typically chosen to be 10%, fraction of atoms being effectively ionized [9]) is determined by the behavior of those initial states of a given principal quantum number  $n_0$  that are most vulnerable to microwave perturbation (the initial sample of atoms having a well defined  $n_0$  is a mixture of different angular quantum numbers in the experiment [8]). To understand the atomic response for higher microwave amplitudes one should consider the atomic states more resistant to perturbation, which ionize at higher  $F$  values and determine the behavior of  $P(F)$ .

The aim of this paper is to provide an analysis of the ionization threshold dependence for the state-specific experiment, i.e., assuming that the atoms are prepared in a well-defined initial state  $(n_0, l_0, m_0)$ . Such complete information is sufficient to understand the  $P(F)$  behavior for an arbitrary initial mixture of states. Since in the studied regime of frequencies the classical simulations reproduce experimental data quite well [8] we limit ourselves here to a classical dynamics picture, determining the thresholds using the Chirikov overlap criterion [10]. We shall in fact limit the discussion here to the simplified 2D model of an atom, restricting the motion of the electron to the polarization plane. Such an approach proved to be quite useful in both classical [11–13] and quantum [2] studies of the ionization in the presence of CP microwaves. Clearly, such a restricted model (assuming the quantization axis to be perpendicular to the polarization plane we can treat the initial states of  $l_0 = m_0$  only) may provide qualitative information only. Still, it may be sufficient to understand the sensitivity of the ionization signal to the microwave polarization.

The results obtained below, while providing some under-

standing of the existing data [8], should be of relevance for future experiments. In particular, they are applicable to possible experiments with initial states of well-defined quantum numbers. Present experimental techniques [14] allow for the preparation of both elongated and circular or elliptic states. Thus it should be possible to prepare quantum states with well-defined quantum numbers before the atoms enter the microwave cavity.

In Sec. II we shall present the classical dynamics analysis of the microwave excitation of H atoms. Applying the Chirikov overlap criterion, we derive the analytic estimate for the onset of unbounded diffusion in action space for atoms illuminated by the microwave field of arbitrary elliptical polarization [Eq. (2.21)]. Provided the microwave field is turned on for sufficiently long times (atoms cross the cavity with sufficiently low velocity) this estimate coincides with the ionization threshold. For shorter interaction times, the estimate provides a lower bound for the microwave amplitude that may result in effective excitation and/or ionization. Using the derived estimate, we discuss in Secs. III and IV the prediction for fields of different polarization (the CP results has been presented in [13]). The analytic prediction is compared with the results of numerical simulations. Section V is devoted to a comparison of our results with the experiment of Bellermann *et al.* [8]. We conclude in Sec. VI.

## II. RESONANCE OVERLAP ANALYSIS

Consider a hydrogen atom perturbed by an elliptically polarized microwave field in the dipole approximation. Restricting the motion of the electron to the polarization plane yields the Hamiltonian (in atomic units) of the 2D system:

$$H = H_0 + FH_1, \quad (2.1)$$

where

$$H_0 = \frac{p_x^2 + p_y^2}{2} - \frac{1}{\sqrt{x^2 + y^2}} \quad (2.2)$$

and

$$H_1 = x \cos \omega t + \alpha y \sin \omega t. \quad (2.3)$$

$F(\omega)$  denotes the amplitude (frequency) of the microwave radiation, while  $\alpha$  determines the degree of ellipticity. In particular,  $\alpha=0$  corresponds to a linear polarization, while  $\alpha=1$  corresponds to a circular polarization of the microwave field. The EP field may be decomposed into two CP waves rotating in the opposite sense:

$$H_1 = \frac{1+\alpha}{2}(x \cos \omega t + y \sin \omega t) + \frac{1-\alpha}{2}(x \cos \omega t - y \sin \omega t), \quad (2.4)$$

which allows us to express the Hamiltonian in the action-angle variables by directly transposing the expressions valid for a CP case [11,13],

$$H(\theta, J, \phi, L, t) = H_0(J) + FH_1, \quad (2.5)$$

where

$$H_0(J) = -\frac{1}{2J^2}, \quad (2.6)$$

$$H_1(\theta, J, \phi, L, t) = \frac{1+\alpha}{2} \sum_{n=-\infty}^{\infty} V_n(J, L) \cos(n\theta + \phi - \omega t) + \frac{1-\alpha}{2} \sum_{n=-\infty}^{\infty} V_n(J, L) \cos(n\theta + \phi + \omega t), \quad (2.7)$$

with

$$V_0(J, L) = -\frac{3e}{2} J^2, \quad (2.8)$$

$$V_n(J, L) = \frac{1}{n} \left[ \mathcal{J}'_n(ne) + \frac{L}{Je} \mathcal{J}_n(ne) \right] J^2 \quad \text{for } n \neq 0 \quad (2.9)$$

and

$$e = \sqrt{1 - \frac{L^2}{J^2}}. \quad (2.10)$$

In Eqs. (2.5)–(2.10)  $J$  is the principal action (a classical analog of the principal quantum number  $n$ ),  $\theta$  the corresponding angle,  $L$  the angular momentum (which is equivalent to the angular momentum projection on the  $z$  axis for the 2D case studied) with the conjugate angle  $\phi$  (which is the angle between the  $x$  axis and the Runge-Lenz vector  $\vec{A}$ ).  $\mathcal{J}_n(x)$  and  $\mathcal{J}'_n(x)$  are the Bessel function and its derivative, respectively, while  $e$  stands for the eccentricity of the initial orbit.

The pure Coulombic motion is characterized by the Kepler frequency

$$\dot{\theta} = \omega_K = \frac{\partial H_0}{\partial J} = \frac{1}{J^3}, \quad (2.11)$$

while

$$\dot{\phi} = \frac{\partial H_0}{\partial L} = 0, \quad (2.12)$$

reflects the conservation of the Runge-Lenz vector in the Coulomb problem. The primary resonances for the perturbed motion satisfy

$$m\theta + \phi - \omega t = \text{const} \quad (2.13)$$

for the first part of the perturbation [Eq. (2.7)] and

$$k\theta + \phi + \omega t = \text{const} \quad (2.14)$$

for the second part [proportional to  $(1-\alpha)/2$ ]. Equations (2.11) and (2.12) indicate that the above resonance conditions are satisfied simultaneously, i.e., for  $J = J_m = (m/\omega)^{1/3}$  the  $m:1$  resonance occurs due to the first part of the perturbation while the second resonance condition is met for  $k = -m$ ,  $J_k = J_m$ . Note that for positive  $m$ , the first resonance corresponds to the electronic motion rotating around

the nucleus in the same sense as the first CP wave in Eq. (2.4). Then the condition  $k = -m < 0$  signifies that the electron rotates in the opposite sense to the second CP wave in Eq. (2.4). We have called the former situation a ‘‘corotating’’ resonance, while the latter was a ‘‘counterrotating’’ resonance in the previous analysis of CP microwave field ionization [13]. Let us immediately recall here that for low-eccentricity orbits the corotating resonances strongly affect the electronic motion, while when the field rotates in the opposite direction from the electron, the atom is more resistant to the perturbation [13]. This will have important consequences below.

Let us apply now the secular perturbation theory around a given  $m:1$  resonance. A canonical transformation to slowly varying variables  $\hat{J} = J/m$  and  $\hat{\theta} = m\theta - \omega t$  allows us to average the perturbation over the remaining fast time variable. Such an approach is valid up to first order in  $F$ . Expanding simultaneously  $H_0$  around the resonance value of the principal action  $\tilde{J} = \hat{J} - \hat{J}_m$  and leaving the terms quadratic in  $\tilde{J}$  yields the approximate resonance Hamiltonian

$$\begin{aligned} \mathcal{H}_m = & -\frac{3}{2m^2\hat{J}_m^4}\tilde{J}^2 + F\frac{1+\alpha}{2}V_m(\hat{J}_m, L)\cos(\hat{\theta} + \phi) \\ & + F\frac{1-\alpha}{2}V_{-m}(\hat{J}_m, L)\cos(\hat{\theta} - \phi). \end{aligned} \quad (2.15)$$

It is crucial to realize that while the resonance island motion is described by  $\tilde{J}$  and the conjugate variable  $\hat{\theta}$ , the remaining variables  $L, \phi$  are conserved (approximately, up to the first order in  $F$ ) and characterize the initial orbit (compare also the discussion in [8]). In particular,  $L$ , via the eccentricity  $e$ , describes the orbit’s shape, while  $\phi$  (being an angle between the  $x$  axis and the Runge-Lenz vector) describes its orientation. Of course, on a long time scale  $\phi$  changes leading to the precession of the electronic trajectory. Close to the center of the resonance island, where changes of  $\hat{\theta}$  are small, one can perform a further average over  $\phi$  to get an integrable pendulum approximation for the effective secular motion. However, our aim here is quite an opposite one: we are interested in the motion close to the borders of the resonance island, where the overlap with the nearby resonances occurs.

Thus  $\phi$  and  $L$  may be considered as approximately conserved quantities, i.e., the parameters describing the initial trajectory. The effective Hamiltonian, (2.15) may be expressed as

$$\mathcal{H}_m = -\frac{3}{2m^2\hat{J}_m^4}\tilde{J}^2 + F\Gamma_m(\hat{J}_m, L, \phi; \alpha)\cos(\hat{\theta} - \beta), \quad (2.16)$$

where  $\beta$  is a constant (up to the first order in  $F$ ) and may be incorporated into  $\hat{\theta}$  by the shift of the origin while

$$\begin{aligned} \Gamma_m(\hat{J}_m, L, \phi; \alpha) = & \left[ \left( \frac{1+\alpha}{2}V_m \right)^2 \right. \\ & + 2\cos 2\phi \frac{1+\alpha}{2}V_m \frac{1-\alpha}{2}V_{-m} \\ & \left. + \left( \frac{1-\alpha}{2}V_{-m} \right)^2 \right]^{1/2}. \end{aligned} \quad (2.17)$$

The width of the resonance island is given as  $\Delta_m = 4m^2\hat{J}_m^2\sqrt{F\Gamma_m/3}$  [11]. Apart from the typical square-root dependence on the perturbation strength represented by the amplitude of the microwave field  $F$ , all the information about the interaction is contained in  $\Gamma_m$ . A comparison of Eqs. (2.15)–(2.17) indicates that the electron is in resonance simultaneously with two waves, with strengths of the interaction being characterized by  $(1+\alpha)V_m/2$  and  $(1-\alpha)V_{-m}/2$ , respectively. Both waves are coupled to each other, the coupling strength being determined by the orientation of the electronic motion ellipse as given by  $\phi$ , i.e., the angle between the  $x$  axis and the Runge-Lenz vector. The relevant range of changes in  $\phi$  is the  $[0, \pi/2]$  interval, which manifests itself in the form of  $\Gamma_m$ .

Following Eq. (2.17),  $\Gamma_m$  may be represented geometrically as the length of the vector  $\Gamma_m = |\vec{a} + \vec{b}|$ , where  $\vec{a}$  describes the ‘‘first’’ wave  $|\vec{a}| = (1+\alpha)V_m/2$  and  $\vec{b}$  represents the ‘‘second’’ wave  $|\vec{b}| = (1-\alpha)V_{-m}/2$ , the angle between both vectors being  $2\phi$ . In particular, for  $\phi = 0$  (corresponding to the situation when the Runge-Lenz vector is parallel to the  $x$  axis, i.e., the direction of the large axis of the microwave polarization ellipse), the contributions of both resonances add constructively

$$\Gamma_m = \frac{1+\alpha}{2}V_m + \frac{1-\alpha}{2}V_{-m}. \quad (2.18)$$

For  $\phi = \pi/4$ ,

$$\Gamma_m = \sqrt{\left[ \frac{1+\alpha}{2}V_m \right]^2 + \left[ \frac{1-\alpha}{2}V_{-m} \right]^2}, \quad (2.19)$$

while for  $\phi = \pi/2$ , resonances act *destructively*

$$\Gamma_m = \left| \frac{1+\alpha}{2}V_m - \frac{1-\alpha}{2}V_{-m} \right|. \quad (2.20)$$

Therefore, the effective strength of the perturbation is strongly dependent on the orientation of the electronic ellipse. For the CP microwave field ( $\alpha = 1$ ) the second wave vanishes and the former results [13] are reproduced.

Having prepared the stage, we are now ready to apply the Chirikov overlap criterion to estimate the ionization thresholds in our system. Before doing so, one should realize that the original system studied, even in two dimensions, has five-dimensional phase space due to the explicit time dependence of the Hamiltonian, (2.1). Thus the Kolmogorov-Arnold-Moser (KAM) tori do not divide the phase space and the unbounded Arnold diffusion [15] is present in the system even if the resonances do not overlap. The Chirikov overlap criterion yields the threshold for the diffusion ‘‘across the

resonances,” whereas the Arnold diffusion “along the resonances” appears for arbitrarily small microwave amplitudes. However, the Arnold diffusion is quite slow [15]; moreover, it slows down considerably in the vicinity of KAM tori [16]. Thus one should not expect it to lead, by itself, to high excitation (ionization) in realistic time intervals. Classical ionization (occurring for several hundreds of microwave periods in experiments [8]) may thus be due only to diffusion across the resonances, the threshold for which may be estimated by the Chirikov overlap criterion.

Applying the criterion to two neighboring  $m:1$  and  $m+1:1$  resonances, together with the heuristic “ $2/3$ ” rule [10,15,11,13], we obtain for the threshold microwave amplitude the analytic estimate

$$F_{m,m+1}(L, \phi; \alpha) = \frac{[(m+1)^{1/3} - m^{1/3}]^2}{3[(m+1)^{2/3} \sqrt{\Gamma_{m+1}} + m^{2/3} \sqrt{\Gamma_m}]^2} \omega^{2/3}. \quad (2.21)$$

The above prediction is the lower bound for the unbounded diffusion starting in  $J$  somewhere on the border between the  $m$ th and the  $(m+1)$ th resonance. The bound depends on both the properties of the initial electronic orbit (its eccentricity  $e$ , or rather  $L$  and its orientation in the real space as given by  $\phi$ ) and the ellipticity of the incoming microwave radiation (as determined by  $\alpha$ ). Typically in experiments the ionization thresholds are higher than the bound determined by the onset of the chaotic motion, even in the frequency range where quantum localization [6] plays no role and classical and quantum theoretical simulations agree. This is due to a finite interaction time in simulations and in experiments [17]. On the other hand, close to the onset of the chaotic motion, the diffusion is slow due to bottlenecks to transports, such as cantori [18], and very long times are required for the ionization to occur.

In the following sections we shall compare the predictions coming from the analytical estimate for the threshold [Eq. (2.21)] with the results of numerical simulations for different initial atomic states and different microwave polarizations. This will allow us to gain some insight into the recent experimental results [8]. We shall limit the discussion to the experimental frequency range [8] around the primary resonance. The onset of the ionization will be determined by the field amplitude at which  $m=1$ , i.e., the 1:1 resonance, and  $m=2$ , i.e., the 2:1 resonance, begin to overlap.

### III. LINEAR POLARIZATION

We begin our discussion with the frequently studied case of linear polarization. Figure 1 presents the onset of chaos prediction based on the estimate, (2.21) for different initial orientations of the Kepler ellipse (as indicated by the values of  $\phi$  in the figure) for different values of the initial angular momentum  $L_0$ . The results are rescaled to  $J=1$ , so  $L_0 \in [0,1]$ . For the initial state with principal action  $J=n_0$  the horizontal axis should be multiplied by  $n_0$ . Similarly, the microwave amplitude is expressed as a scaled field  $F_0 = F n_0^4$ . The corresponding scaled Chirikov overlap prediction value [Eq. (2.21)] is denoted as  $F_c$  in the following.

As expected, the initial orbits elongated parallel to the microwave polarization ( $\phi=0$ ) have the lowest diffusion

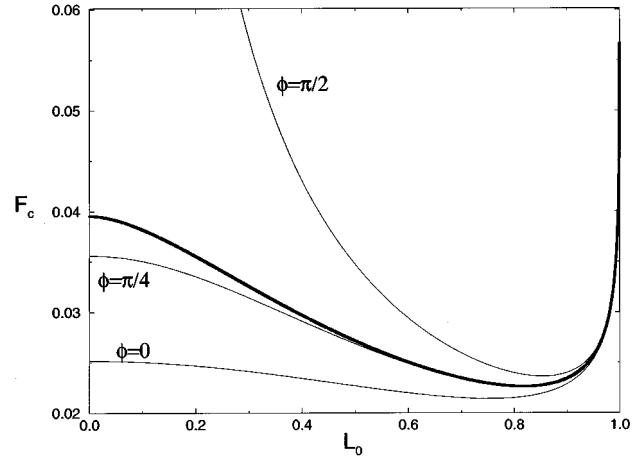


FIG. 1. Critical scaled field value  $F_c$  [Eq. (2.21)] as a function of the scaled angular momentum  $L_0$  for LP microwave excitation. The thick line gives the result obtained from the Hamiltonian averaged over  $\phi$ ; other curves correspond to chosen  $\phi$  values as indicated in the figure. The initial configurations elongated parallel to the polarization axis are most susceptible to perturbation. All curves show a minimum around  $L_0 \approx 0.8$ , thus states of eccentricity  $e \approx 0.6$  are the first to ionize.

threshold for all initial eccentricities ( $e = \sqrt{1-L_0^2}$ ). For such oriented orbits, however, the threshold is not very sensitive to  $L_0$  at least for  $L_0 < 0.8$ . Surprisingly, the highest-eccentricity orbits ( $L_0 \approx 0$ ) do not have the lowest diffusion threshold; the shallow minimum appears around  $L_0 = 0.7$ , corresponding to the eccentricity  $e \approx L_0$ . For low eccentricity, in almost circular states, the threshold rises rapidly, indicating that these states do not contribute to the ionization yield a close to experimentally measured 10% thresholds.

The difference between the minimum threshold and its value for lower  $L_0$  is quite small. This explains why one-dimensional models [1,6] may yield a reasonable prediction for the ionization onset. However, it is apparently not correct to say that the high eccentricity states elongated parallel to the polarization axis are most susceptible to the perturbation. It is appropriate to mention here that the recently obtained exact quantum results for the 3D atom in the same frequency range [19] point in the same direction. Clearly, the validity of the one-dimensional model to describe the ionization process in linear polarization should be reexamined in a broader frequency range [20].

For initial orbits inclined with respect to the polarization axis, the minimum of the threshold becomes more pronounced and shifts to lower eccentricity states. For such orbits the Chirikov overlap threshold rises rapidly with eccentricity for  $e$  sufficiently large. This is due to both the destructive effect of two waves rotating in the opposite directions [compare Eq. (2.20)] and the fact that as  $L_0 \rightarrow 0$ ,  $V_m$  and  $V_{-m}$  become equal. In effect, the Chirikov criterion based on the effective Hamiltonian correct up to first order in  $F$  predicts that  $L_0=0$  orbits perpendicular to the polarization axis ( $\phi = \pi/2$ ) are stable against the perturbation.

To see the typical average behavior, for orbits of different orientations  $\phi$  one may use the resonance pendulum Hamiltonian obtained by averaging Eq. (2.16) over  $\phi$ . The threshold values obtained from such an approach show also a pro-

nounced minimum for  $L_0 \approx 0.8$  (thick line in Fig. 1). This minimum practically coincides with the diffusion threshold for  $\phi=0$ ,  $L_0=0$  orbits, i.e., for the one-dimensional model of a H atom.

The predictions presented in Fig. 1 are compared with the results of classical simulations as shown in Fig. 2. For the latter we assumed the flat-top microwave pulse of the form

$$f(t) = \begin{cases} \sin^2(\pi t/2\tau) & \text{for } t < \tau \\ 1 & \text{for } \tau < t < T - \tau \\ \cos^2[\pi(t - T + \tau)/2\tau] & \text{for } T - \tau < t < T. \end{cases} \quad (3.1)$$

While in the EP microwave experiment [8] a half-sine pulse is used, the flat-top pulse better corresponds to LP experiments [1]. Typically we assume  $\tau=25$  microwave cycles.

Figure 2(a) shows the ionization probability for orbits elongated parallel to the field ( $\phi=0$ ) as a function of  $L_0$  for two different pulse durations  $T$ . In both cases the behavior predicted by the overlap formula, Eq. (2.21) and depicted in Fig. 1 is reproduced qualitatively. Namely, the ionization yield obtained is not sensitive to  $L_0$  for  $L_0$  small and then sharply drops to zero for almost circular orbits. However, in a finite time simulation, the transition to ‘‘excitation resistant’’ states occurs around  $L_0=0.5$  and is significantly shifted with respect to the  $L_0=0.7$  prediction coming from the Chirikov criterion. This may be due to a finite interaction time as well as to the fact that in simulations we study the ionization yield for a fixed microwave amplitude and not the absolute threshold. Note that a higher ionization yield corresponds to a lower ionization threshold since, in most cases, the ionization yield is classically an increasing function of  $F$ . However, the dependence of the yield  $P$  on  $F$  may be dependent on  $L_0$ . Therefore, the 10% threshold, i.e., the amplitude  $F$  value when the yield,  $P$  is 10%, may show a slightly different dependence on  $L_0$  from the absolute threshold. The determination of the real ionization threshold for a given finite time would require determination of very low ionization probabilities. To obtain then a statistically significant result, a prohibitively large number of trajectories would be necessary. Thus a comparison with the overlap prediction may be only qualitative (also, a finite  $T$  in simulations makes a quantitative comparison virtually impossible, as mentioned above). For that reason we restrict ourselves mostly to comparisons of ionization yields.

Figure 2(b) shows the numerically obtained yield for states elongated perpendicular to the polarization axis. Note that no ionization yield is obtained for high-eccentricity (low  $L_0$ ) states even for the quite high  $F_0$  value assumed in the simulation. The yield drops for almost circular states, the overall behavior being in qualitative agreement with the corresponding curve from Fig. 1.

Figure 2(c) shows the ionization yields for initial samples not preselected with respect to the ellipse orientation. Thus they correspond to the thick line prediction in Fig. 1 obtained by averaging over  $\phi$ . Again observe the qualitative agreement of the numerical results with the theoretical prediction: a maximum yield occurs for states of medium eccentricity for all assumed microwave amplitude values. As previously

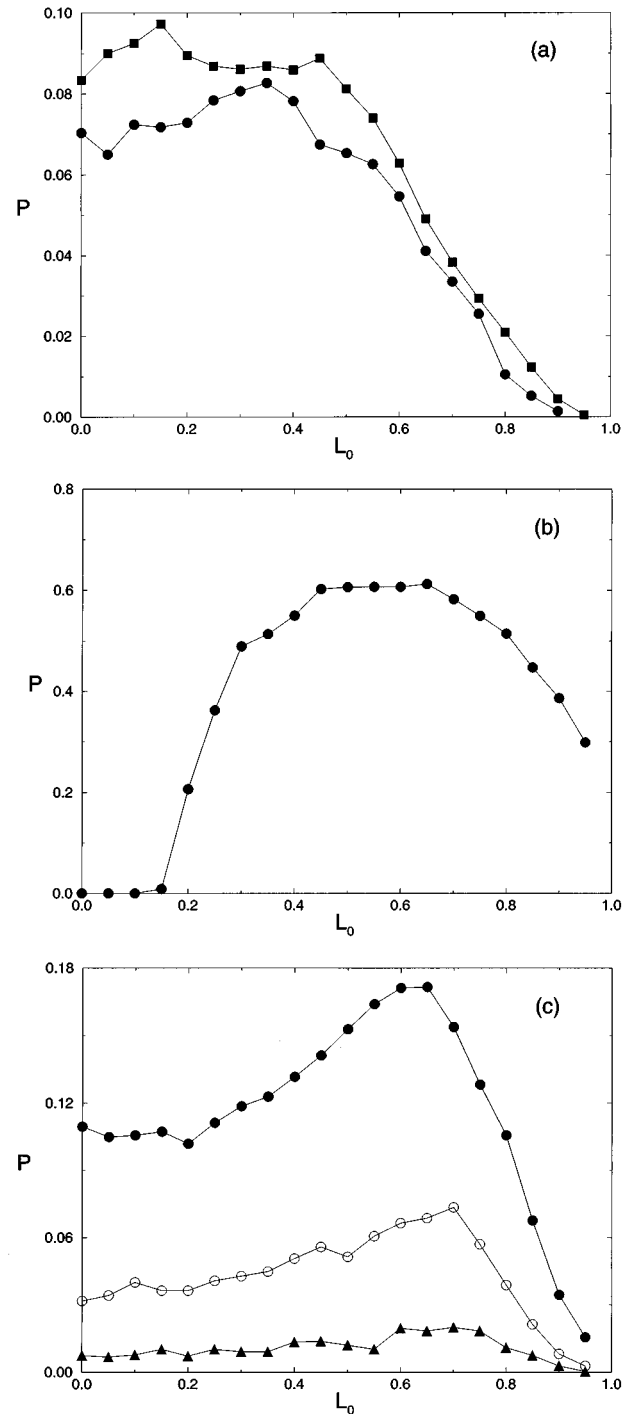


FIG. 2. Ionization yield  $P$  as a function of scaled angular momentum of the initial orbits  $L_0$  for different orientations of orbits with respect to the LP axis. (a)  $\phi=0$ ,  $\omega_0=1.2$ . Circles correspond to a pulse of duration  $T=100$  microwave cycles and  $F_0=0.06$ , while squares correspond to  $T=300$  and  $F_0=0.036$ . In both cases the initial sample consisted of  $10^4$  trajectories. Note that all orbits with  $L_0 < 0.4$  lead to a comparable ionization yield. (b)  $\phi=\pi/2$ ,  $F_0=0.08$ , and  $T=300$ . Even when a large yield is obtained for orbits of large  $L_0$ , orbits elongated perpendicular to the polarization axis do not ionize. (c) Data for initial microcanonical sample (all values of  $\phi$  are allowed):  $\omega_0=1.2$ ,  $T=300$ , and  $F_0=0.045$ ,  $0.038$ , and  $0.033$  for filled circles, open circles, and triangles, respectively. Note that orbits of medium eccentricity give the largest ionization yield.

one may observe a slight shift of the optimal yield with respect to the position of the minimum threshold in the theoretical predictions.

#### IV. ELLIPTICALLY POLARIZED MICROWAVES

When the polarization of microwaves is not linear, the strength of the interaction between the field and the electron depends on the mutual orientations of the direction of rotation of the electron on its orbit and the direction of rotation of the microwave amplitude. The simplest situation occurs for CP microwaves when only one ( $\alpha=1$ ) of the two waves in Eq. (2.4) is present. For completeness let us recall here [12,13] that if the electron rotates in the same direction as the field it is much more vulnerable to perturbation and the threshold for the ionization is then much lower than for the opposite case. A transformation from one such situation to the other may be realized by changing the sign of  $\omega$  or, equivalently, that of  $L$ . As discussed in detail in [13], this asymmetry is directly related to an asymmetry of values of  $V_n(J,L)$  [Eq. (2.9)] with respect to the  $n \rightarrow -n$  (or, equivalently,  $L \rightarrow -L$ ) transformation. We referred to the resonances occurring for the field and the electron rotating in the same direction as corotating (those are strong resonances, occurring for  $\omega L > 0$ ) and the resonances occurring for  $\omega L < 0$  as counterrotating [13].

For a general EP case, as discussed in Sec. III, the electron is in resonance simultaneously with two CP waves of opposite helicity, i.e., one of these resonances is of the corotating type while the other is of the counterrotating type. The corresponding  $V_n(J,L)$  coupling terms in the Fourier expansion (2.7) are multiplied by  $(1 \pm \alpha)/2$  coefficients. For the LP case, considered in Sec. III,  $\alpha=0$  and both terms come with equal weights. Then, as expected, the sign of  $\omega$  (or  $L$ ) plays no role.

In the following we shall assume that  $\alpha \in [0,1]$  and  $\omega > 0$ . Then the electronic orbits with  $\omega_K \approx \omega$  and  $L > 0$  will be in a strong, corotating resonance with the field, the resonant Fourier expansion coefficient being  $(1 + \alpha)V_1(J,L)/2$  and the effect of the counter-rotating resonance being small due to both the  $(1 - \alpha)/2$  factor and the fact that  $V_{-1} < V_1$  for  $L > 0$  [13]. On the other hand, for  $L < 0$ , the difference in strength of the  $V_{\pm 1}$  ( $V_{-1} > V_1$ ) terms may be partially canceled by the  $(1 \pm \alpha)/2$  terms. This may lead to a great variety of possible behaviors of the diffusion threshold field value as a function of  $L$ , the orientation of the electronic ellipse with respect to the main axis of the microwave polarization ellipse (as given by  $\phi$ ; compare Sec. II).

Figure 3 presents the thresholds for  $L > 0$  in the  $L_0$ - $\phi$  plane (numerical data are presented in scaled variables as before). The threshold surface is symmetric around  $\phi = \pi/2$  and the range up to  $\pi$  is plotted for better visualization of the surface. For all values of  $\alpha$  (as indicated in the figure), the lowest threshold value, for a given  $L_0$ , is obtained for  $\phi = 0$ . The sensitivity of the threshold to changes of  $\phi$  is the biggest for high-eccentricity (low  $L_0$ ), strongly elongated orbits. This is easy to understand: the electron moving on a very elongated ellipse (degenerating into a line for  $L_0 = 0$ ) “feels” mostly the microwave field component polarized in the direction of its major axis (the Runge-Lenz vector). On the other hand, the circular orbits are insensitive to  $\phi$ . Note

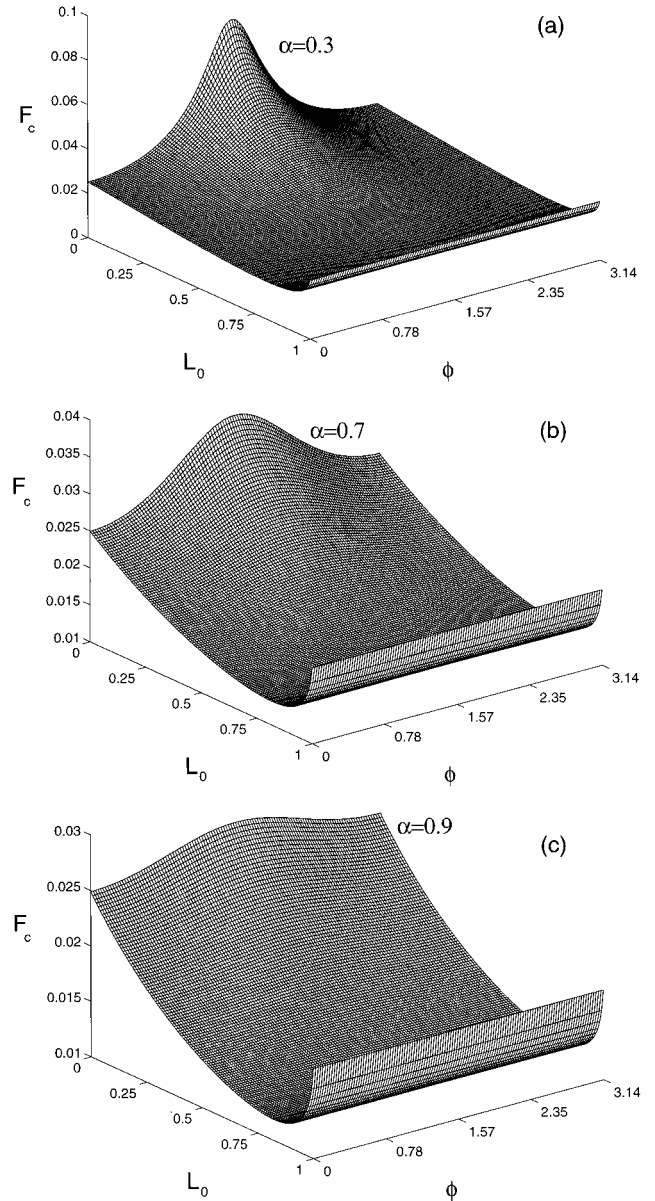


FIG. 3. Chirikov overlap prediction for the onset of unbounded diffusion in the plane spanned by  $\phi$  and the scaled angular momentum  $L_0$  (for  $L_0 > 0$ ). The values of parameter  $\alpha$  determining the ellipticity of the microwaves are indicated in each panel.

that for all  $\alpha$  values (the degree of ellipticity of the microwave polarization) orbits of medium eccentricity have the lowest threshold for unbounded diffusion. Following the line  $\phi = 0$  for different  $\alpha$  values in Fig. 3 it is easy to notice that the minimal  $F_c$  value occurs for  $L_0 \approx 0.8$  for arbitrary  $\alpha$ .

Typically, for  $L_0 < 0$  the thresholds, as predicted by Eq. (2.21), lay significantly higher than for  $L_0 > 0$ , as shown for a few small  $\phi$  values in Fig. 4. This is expected from the discussion presented above; for  $L_0 < 0$ , the leading terms  $V_{-1}$  and  $V_{-2}$  and are multiplied by  $(1 - \alpha)/2$  thus the widths of the resonance islands grow slower than for  $L_0 > 0$ . Surprisingly, however, when one allows  $\phi$  to take all possible values (Fig. 5), a spectacular, double-peak stability region centered around  $\phi = \pi/2$  is revealed. The eccentricity of the orbits corresponding to the stability region depends strongly

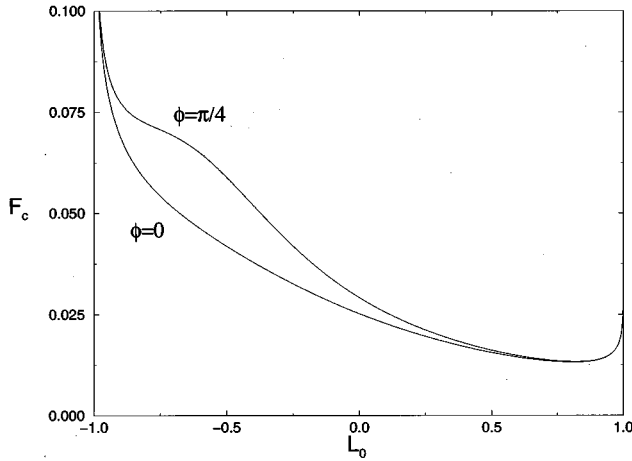


FIG. 4. Chirikov overlap prediction for both positive and negative  $L_0$  in EP microwaves of  $\alpha=0.7$  for orbits whose main axis is close to the main axis of the polarization ellipse. The values of  $\phi$  are indicated in the figure. Notice that orbits with  $L_0 < 0$  require higher microwave amplitudes for the overlap to occur.

on the degree of the microwave field ellipticity  $\alpha$ ; compare the plots in Fig. 5.

The stability has a quite simple origin, although its appearance seems to be, at first glance, quite unexpected. Consider again Eq. (2.17), which gives the width of a given resonance island, and in particular Eq. (2.20), corresponding to  $\phi = \pi/2$ . The contribution of two waves to the resonance island act destructively there. Since, for  $L_0 < 0$ ,  $V_{-m} > V_m$  for  $m > 0$ , there exists an  $\alpha$  value (dependent on the resonance number  $m$  and the angular momentum  $L_0$ ) where the two terms cancel, leading to the vanishing width of the island. At the cancellation point, the threshold value obtained from the Chirikov criterion is maximal. For the overlap between 1:1 and 2:1 resonance zones, for a given  $\alpha$ , the width of the 1:1 resonance shrinks to zero at a different value of  $L_0$  from that of the 2:1 resonance island (compare Fig. 6), resulting in the double-peak structure in Fig. 5.

The question remains, however, whether the stability region discussed above is an artifact of the Chirikov overlap criterion analysis valid in first order in  $F$ . The results of the numerical simulations, performed for several  $\alpha$  values, indicate that indeed the stability region exists and its position is well correlated with the predictions of Eq. (2.21); compare Fig. 7. As could be expected, the Chirikov criterion overestimates the stability of the motion in this case. After all the estimation of the resonance island is based on the expansion in  $F$  in first order. The disappearance of the island in first order does not preclude existence of the real island up to all orders in  $F$ . The primary resonance becomes the secondary resonance with an understandably smaller width. It would be most interesting to extend the analysis to higher-order resonances to get an analytic prediction for the threshold in this region, but this is beyond the scope of the present paper.

To complete the presentation of the EP case, we show in Fig. 8 the thresholds obtained by averaging the Hamiltonian over  $\phi$  together with the results of the appropriate numerical simulations. Keeping in mind that the high numerical ionization yield corresponds to a low threshold value (much lower than the value of  $F$  used in the simulation), i.e., that theoret-

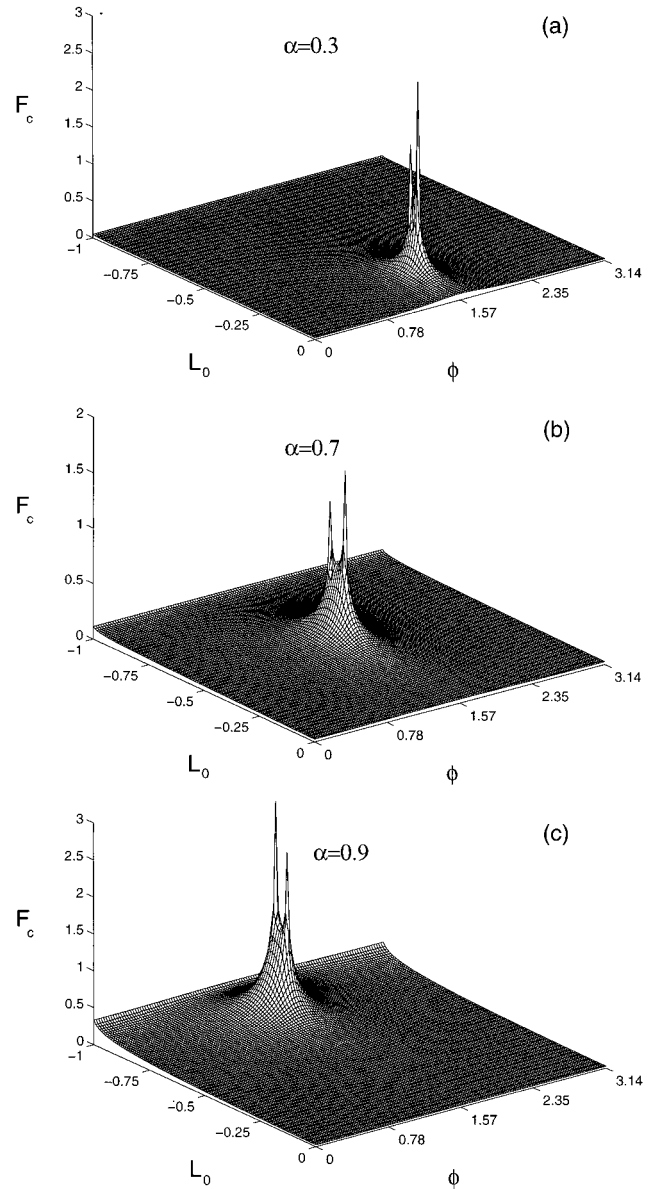


FIG. 5. Same as Fig. 3, but for  $L_0 < 0$ . Values of  $\alpha$  are indicated in each panel. Notice double-peak structures, indicating an increased stability of the orbits for the corresponding initial conditions. For a discussion see the text.

ical and numerical simulation curves may be roughly compared if the numerical result is reflected with respect to the horizontal axis, the corresponding curves show nice qualitative agreement. This indicates again that the Chirikov criterion captures the essential features of the ionization threshold.

## V. IONIZATION THRESHOLDS FOR THE MICROCANONICAL SAMPLE

After studying in detail the onset of diffusive excitation for different, well-defined initial states, it is now possible to relate the predictions based on Eq. (2.21) to the results of recent experiment of Bellerma *et al.* [8]. As mentioned in the Introduction, in the experiment, atoms entering the cavity have a well-defined principal quantum number  $n_0$ . However,

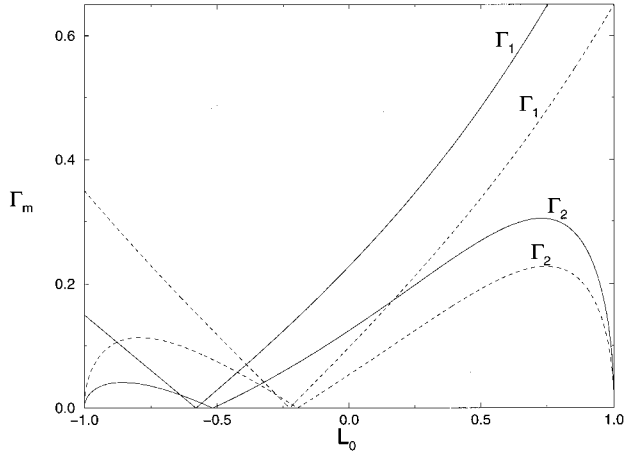


FIG. 6. Widths of the resonances (denoted in the figure) as a function of  $L_0$  for  $\alpha=0.7$  (full lines) and  $\alpha=0.3$  (dashed lines). Note that the minima of resonances widths weakly depend on the resonance order.

the sample is a mixture of different angular momentum states. The atoms interact with a half-sine-shaped microwave pulse (while passing through the cavity) of a duration of 153 microwave cycles. Clearly, this is not a situation suitable for the quantitative comparison with the predictions of the Chirikov overlap criterion. For the latter, a flat-top, very long pulse would be more appropriate.

Still, it may be worthwhile to compare qualitatively the experimental results (as well as 3D classical simulations that, according to [8], reproduce quite well the experimental data) with the Chirikov overlap estimates. The latter may be obtained based on Eq. (2.21) which yields the onset of diffusive excitation for a trajectory with a given  $L$  and  $\phi$ . Since in a 2D atom all  $L$  values are equally probable, similarly to all  $\phi$  values, it is a straightforward procedure to find the micro-

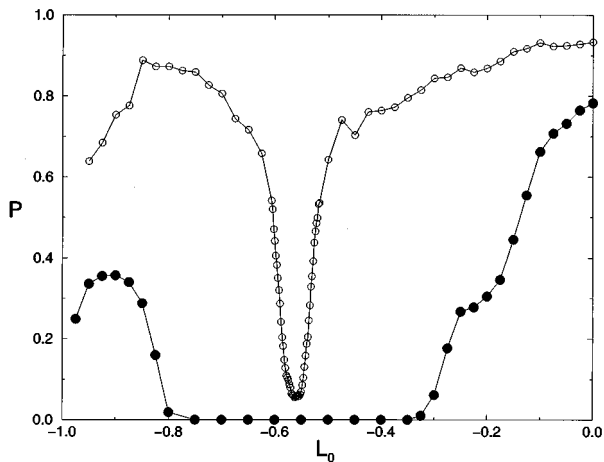


FIG. 7. Ionization yield as a function of  $L_0$  for orbits oriented perpendicular ( $\varphi = \pi/2$ ) to the main axis of EP field with  $\alpha=0.7$ . The flat top pulse of duration  $T=300$  cycles and  $\omega_0=1.2$  was applied to 5000 initial conditions. Filled circles correspond to  $F_0=0.09$ , open circles to  $F_0=0.19$ . Observe the narrow minimum corresponding to the stable double-peaked structure in Fig. 5. For finite times and due to the statistical errors for a finite sample the splitting into the doublet cannot be observed.

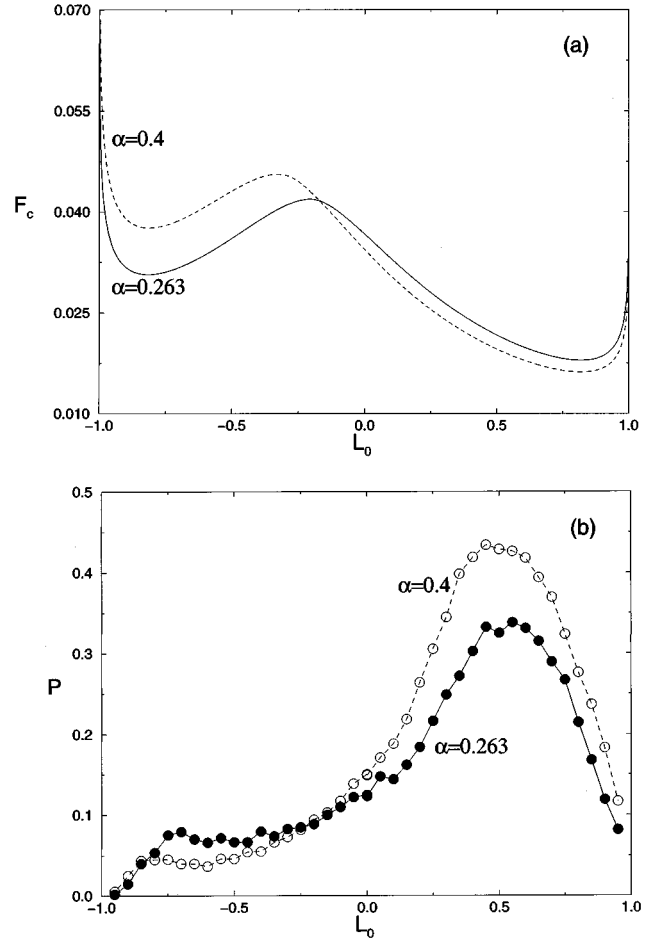


FIG. 8. Comparison of (a) the overlap prediction with (b) results of numerical simulations for samples averaged over possible orientations of electronic orbits (i.e., over  $\phi$ ); both are represented as a function of the initial  $L_0$ . The ellipticity parameter  $\alpha=0.263$  corresponds to experimental data of [8]. In numerical simulations  $F_0=0.045$ , the pulse duration  $T=300$  and  $\omega_0=1.2$ . Note that the maximal yield [in (b)] nicely corresponds to the minimal threshold value in (a). States of medium eccentricity with  $L\omega > 0$  are most susceptible to perturbation and determine the threshold for the microcanonical initial sample.

wave amplitude for which the threshold is reached for a given  $s\%$  of the microcanonically distributed sample, while the remaining part of the sample is still below the corresponding threshold. This will then be interpreted as the Chirikov overlap prediction for the  $s\%$  ionization yield (assuming a very long interaction time).

Let us note that the approach outlined above is different from the application of the Chirikov overlap criterion used in [8]. The authors of [8] found the threshold field by determining the minimum of the overlap with respect to all possible trajectories in the microcanonical sample. Since the Chirikov criterion may yield the qualitative estimate of the experimental threshold only (for the reasons stated above), the simpler approach of [8] is fully justified for the threshold determination. However, this approach cannot give predictions concerning the dependence of the ionization yield on the microwave field value and its polarization, while our procedure yields also this information.

Rather than giving the absolute microwave scaled field

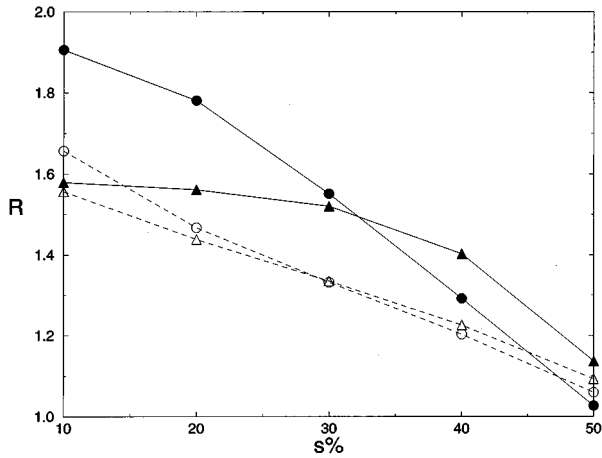


FIG. 9. Ratio of the LP microwave amplitude to the CP microwave amplitude, both leading to  $s\%$  ionization yield, denoted as  $R_L$ , and a similar ratio for EP microwaves, with  $\alpha=0.263$ , to the CP amplitude  $R_E$  as a function of  $s\%$ . Full circles (triangles) correspond to  $R_L$  ( $R_E$ ) obtained from the Chirikov overlap criterion, while open symbols represent the results obtained numerically for the half-sine microwave pulse with a duration of  $T=153$  microwave cycles, frequency  $\omega_0=1.2$ , and the cutoff  $n_c=110$  [8]. The difference between the two reflect the dependence of the diffusion speed on the microwave polarization.

values corresponding to a given  $s\%$  yield for different polarizations of the microwaves as coming from our Chirikov overlap analysis, we plot their ratio in Fig. 9. Denote by  $R_L(s\%) = F_0^{\text{LP}}(s\%)/F_0^{\text{CP}}(s\%)$  the ratio of the scaled LP microwave amplitude leading to  $s\%$  yield according to the Chirikov prediction to the corresponding amplitude for the CP field. Similarly set  $R_E(s\%) = F_0^{\text{EP}}(s\%)/F_0^{\text{CP}}(s\%)$ , where  $\alpha=0.263$  as in [8] for the EP microwave field. It has been found experimentally that  $R_L(10\%)=1.41$  and  $R_E(10\%)=1.26$ . For larger  $s\%$ ,  $R_L(s\%)$  decreases while  $R_E(s\%)$  remains roughly constant [8]. Our 2D Chirikov overlap analysis consistently overestimates both  $R_L$  and  $R_E$  while rather nicely reproducing the trend with  $s\%$  (compare Fig. 9).

For a comparison we show also in Fig. 9 the results obtained from a fully numerical 2D model simulation for the microwave pulse of the shape and duration closely resembling the experiment [8]. The numerical results are closer to the experimental data [8] than the Chirikov overlap estimates. That suggests the difference in the chaotic diffusive transport above the onset of the chaotic motion occurring for LP and CP cases. Specifically since  $R_L$  is higher for the onset of diffusive motion than for a finite time simulation, we conclude that the diffusion just above the threshold for the CP case is considerably slower than the diffusion occurring for the LP case. This suggests that the remnants of regularity acting as bottlenecks for transport are more important in the CP case. The remaining differences between our simulations in two dimensions and the experimental results and the 3D simulations of [8] may be due to the reduced dimensionality in our approach.

The results of the previous sections make it easy, on the other hand, to interpret the behavior of  $R_L$  and  $R_E$  as a function of  $s\%$ . Recall that the threshold field value strongly depends on the direction of rotation of the electron on its

ellipse and the helicity of microwaves. The strongest difference appears for the CP case [12,13] when the corotating resonances overlap for much weaker fields than the counter-rotating ones. In the initial microcanonical sample, half of it corresponds to initial orbits rotating in the same direction as the field, while the other half rotates in the opposite sense and is weakly perturbed by the microwave field which leads to ionization of the other half. Obviously, there is no such difference in the LP case. In effect, to get, say, 30% ionization in a CP case, one must ionize 60% of the corotating half of the sample, while in the LP case the 30% comes from all the possible trajectories. Stated differently, there are more orbits resistant to perturbation in the CP than in the LP field. In effect, the ionization yield increases with  $F$  more slowly in the CP case than in the LP situation. For the general EP field the situation is somewhat in between two extrema, the CP and LP cases.

## VI. CONCLUSION

Using the Chirikov overlap criterion we have estimated the onset of unbounded chaotic diffusion in the phase space of the hydrogen atom irradiated by the microwave field of elliptic polarization. The obtained analytic prediction [Eq. (2.21)] is valid for an arbitrary polarization of the microwaves and the overlap between any  $m:1$  and  $(m+):1$  resonances. On the other hand, the prediction is obtained by assuming the expansion in the first order in  $F$ . In the discussion that follows we concentrate mainly on the  $m=1$  case for which recent experimental results [8] are available.

We discussed first the LP case showing that the Chirikov overlap criterion predictions indicate that not only quasi-one-dimensional orbits pointing in the direction of the polarization axis are most susceptible to ionization. While 1D and 2D threshold values may agree, the orbits that contribute mostly to ionization may have quite small eccentricity. This indicates that 1D models may oversimplify the physics of the LP microwave ionization of H atoms. Let us mention here again that similar conclusions may be reached based on quantum-mechanical results in the same frequency regime [19]. Clearly, additional studies that will compare quantum and classical results in different frequency regions are needed here especially since the optimal classical approach would utilize the second-order invariant [19] for proper classification of initial orbits. Our results for the CP case [13] indicate, however, that this optimal choice would not affect strongly the conclusions reached here.

Equation (2.21) allows us to study the onset of unbounded diffusion for orbits of different shape (eccentricity  $e$ ) oriented in different ways with respect to the polarization ellipse. The initial orbits most susceptible to perturbation have been identified. At the same time we have found an important family of initial orbits that are resistive to the perturbation. Numerical simulations indicate that the stability is only approximate; still, these orbits ionize at much larger microwave amplitudes than the typical orbits. Interestingly, the eccentricity of “stable” orbits is dependent on the polarization parameter  $\alpha$ . Thus irradiating the microcanonical sample by EP microwaves of sufficiently high amplitude may lead to an almost complete ionization of all atoms except those of the eccentricity related to the polarization of EP

microwaves. This may serve as a crude way of producing atoms in states of a given eccentricity while “destroying” the rest of the microcanonical sample.

Finally, we compared the Chirikov overlap predictions as applied to the microcanonical sample with experimental data [8] providing the explanation of the slower increase of the ionization yield with  $F$  for elliptically and even slower for circularly polarized microwaves. This slower increase is due to the existence of orbits less affected by the microwave field, orbits on which the electron rotates in the direction opposite the microwave field vector. We related the disagreement between the overlap prediction and finite time simula-

tions to the fact that the former is conclusive for very long times only. The discrepancy provides information about the difference in diffusion times in the systems compared.

#### ACKNOWLEDGMENTS

We thank Andreas Buchleitner and Dominique Delande for discussions and Robert Gębarowski for supplying his classical simulation code. K.S. acknowledges the support by the Polish Committee of Scientific Research under Young Researcher Project. J.Z. is supported under Project No. 2P03B03810 by the same committee.

- 
- [1] P. M. Koch and K. A. H. van Leeuwen, *Phys. Rep.* **255**, 289 (1995).
- [2] J. Zakrzewski, R. Gębarowski, and D. Delande, *Phys. Rev. A* **54**, 691 (1996), and references therein.
- [3] P. Fu, T. J. Scholz, J. M. Hettema, and T. F. Gallagher, *Phys. Rev. Lett.* **64**, 511 (1990).
- [4] T. F. Gallagher, *Mod. Phys. Lett. B* **5**, 259 (1991).
- [5] J. A. Griffiths and D. Farrelly, *Phys. Rev. A* **45**, R2678 (1992).
- [6] G. Casati, I. Guarneri, and D. L. Shepelyansky, *IEEE J. Quantum Electron.* **24**, 1420 (1988).
- [7] M. Nauenberg, *Europhys. Lett.* **13**, 611 (1990).
- [8] M. R. W. Bellermand, P. M. Koch, D. R. Mariani, and D. Richards, *Phys. Rev. Lett.* **76**, 892 (1996).
- [9] In the experiment [8], by effective ionization one understands either a genuine ionization or excitation above some critical principal quantum number  $n_c \approx 110$ , which leads to subsequent ionization by the electric field outside the microwave cavity.
- [10] B. V. Chirikov, *Phys. Rep.* **52**, 265 (1979).
- [11] J. E. Howard, *Phys. Rev. A* **46**, 364 (1992).
- [12] R. Gębarowski and J. Zakrzewski, *Phys. Rev. A* **51**, 1508 (1995).
- [13] K. Sacha and J. Zakrzewski, *Phys. Rev. A* **55**, 568 (1997).
- [14] J. C. Day, T. Ehrenreich, S. B. Hansen, E. Horsdal-Pedersen, K. S. Mogensen, and K. Taulbjerg, *Phys. Rev. Lett.* **72**, 1612 (1994), and references therein.
- [15] A. J. Lichtenberg and M. A. Leiberman, *Regular and Chaotic Dynamics*, 2nd ed. (Springer, New York, 1992).
- [16] J. Laskar, *Physica D* **67**, 257 (1993); J. Laskar (unpublished).
- [17] O. Benson, A. Buchleitner, G. Raithel, M. Arndt, R. N. Mantegna, and H. Walther, *Phys. Rev. A* **51**, 4862 (1995).
- [18] R. S. MacKay, J. D. Meiss, and I. C. Percival, *Physica D* **13**, 55 (1984).
- [19] A. Buchleitner and D. Delande, *Phys. Rev. A* **55**, R1589 (1997).
- [20] Extensive classical simulation studies reported by D. Richards, in *Aspects of Electron-Molecule Scattering and Photoionization*, edited by A. Herzenberg, AIP Conf. Proc. No. 204 (AIP, New York, 1990), p. 45, suggest that real 3D atomic motion should be taken into account for large-scaled frequencies. We stress that our results, are obtained near  $\omega/\omega_K \approx 1$ ; see also J. G. Leopold and D. Richards, *J. Phys. B* **19**, 1125 (1986).